DEU FMD 26(78) (2024) 470-480

Dokuz Eylül Üniversitesi Mühendislik Fakültesi Fen ve Mühendislik Dergisi
Dokuz Eylul University Faculty of Engineering Journal of Science and Engineering
Elektronik/Online ISSN: 2547-958X

*RESEARCH ARTICLE / ARAŞTIRMA MAKALESI*

# Modeling Gravity Gradients from Surface Gravity Anomaly Data

## Yüzey Gravite Anomali Verilerinden Gravite Gradyentlerin Modellenmesi

**Sibel Uzun** *

Ondokuz Mayıs Üniversitesi Mühendislik Fakültesi Harita Mühendisliği Bölümü, Samsun, TÜRKİYE
*Corresponding Author / Sorumlu Yazar* *: sibel.uzun@omu.edu.tr

**Abstract**

Gravity gradients are useful to characterize near mass anomalies since they are much more sensitive to short wavelength anomalies than gravitational accelerations. Estimating gravity gradients from surface gravity data is based on numerical implementations of solutions to geodetic boundary value problem for determination of disturbing potential. One of methods to solve this problem is least-squares collocation which is basically based on data and a defined covariance function. This study deals with estimating gravity gradient tensor components from along track surface gravity anomaly data. The Least-Squares Collocation solution is based on a stationary local covariance function defined for the disturbing potential which allows upward continuation of the observations to a desired altitude. The modeling method is evaluated in using Earth Gravitational Model 2008(EGM2008) and real airborne gravity gradiometry data collected over Southern Texas, Oklahoma region. The results show that modeled gravity gradients estimated in both on the ground and at a certain altitude have basically good agreement with EGM08 gradients. Modeled gradients including horizontal components in the east-west direction exhibit some discrepancies in comparison to the airborne gradiometry data, which may be attributed to some measurement errors in the gradient data.

***Keywords:*** *Least-squares collocation, Covariance matrix, Gravity gradient tensor*

**Öz**

Gravite gradyentleri kısa dalga boylu anomalilere yerçekimi ivmelerinden daha fazla duyarlı oldukları için yüzeye yakın kütle anomalilerini belirlemede faydalıdırlar. Gravite Gradyentlerinin yüzey gravite anomalilerinden kestirimi bozucu potansiyelin belirlenmesinde jeodezik sınır değer problemi çözümlerinin sayısal uygulamalarına dayanmaktadır. Bu problemi çözmenin yöntemlerinden birisi temel olarak veriye ve tanımlanan bir kovaryans fonksiyonuna dayanan En Küçük Kareler Kollokasyonudur. Bu çalışma bir profil boyunca verilen yüzey gravite anomali verilerinden gravite gradyent tensör elemanlarının kestirimi ile ilgilidir. En küçük kareler kollokasyon çözümü gözlemlerin istenen bir yüksekliğe yukarı uzanımına imkan veren bozucu potansiyel için tanımlanmış bir durağan yerel kovaryans fonksiyonuna dayanır. Modelleme yöntemi Yer Gravite Modeli 2008 ve Güney Teksas Oklahoma bölgesi üzerinde toplanmış gerçek havadan gravite gradyometri verileri kullanılarak değerlendirilmiştir. Sonuçlar, hem yeryüzü üzerinde hem de belirli bir yükseklikte kestirilen modellenmiş gravite gradyentlerinin EGM08 gradyentleri ile uyumlu olduğunu göstermektedir. Doğu-batı yönündeki yatay bileşenleri içeren modellenmiş gradyentler, havadan gradyometre verilerine kıyasla bazı uyumsuzluklar göstermektedir; bu durum gradyent verilerindeki bazı ölçüm hatalarına bağlı olabilir.

***Anahtar Kelimeler:*** *Ek küçük kareler kollokasyon, Kovaryans matris, Gravite gradyent tensor*

## 1. Introduction

According to Newton's Law of Gravitation, the gravitational acceleration between two mass points attracting each other attenuates with the inverse of squared distance from attracting point to a source point. The spatial derivatives of the gravitational acceleration, namely gravity gradients, attenuate with the cube of inverse distance from the source point. Since derivatives of a function reveal its local properties, the effect of attenuation with altitude is compensated by differentiation [1]. Therefore, gravitational gradients become more sensitive to shallow structure mass anomalies than gravity [1]. As such, they have become useful tool to interpret near subsurface geologic structures. In addition, gradient measuring instruments provide multiple components of full gradient tensor. The use of gravity gradients dates back to the invention of Eotvos torsion balance instrument by Lorand von Eotvos in 1896. The use of instrument was primarily on for oil exploration [2]. With the advent of moving based gravity gradiometer survey system in 1970s, the usage of the gravity gradients in resource exploration has been brought to the fore and found its place in a wide range of application areas. Gravity gradients have been used to detect fault related geothermal resources by [3-4,5]. [6] used a 3D inversion of gravity gradients to explore mineral deposits. [7] explores mineral deposits and geothermal systems from airborne gravity gradiometry data and used tensor invariants to interpret lineaments. [8] have modelled satellite- based gravity gradient data to interpret lithospheric structure. Gravity gradient tensor has been derived from gravity data by [9]. They derived gravity gradient tensor from gravity data using Fourier transform in frequency domain. [10] have derived gravity gradients from satellite altimetry data for bathymetry inversion. [11,12] derived three algorithms based on Stokes integral, Least-Squares collocation and radial basis spline models from both regularly distributed surface gravity anomaly and elevation data in space domain to validate airborne gravity gradiometry survey data.

DOI: https://doi.org/10.21205/deufmd.2024267813

Geliş Tarihi / Received: 16.10.2023
Kabul Tarihi / Accepted: 31.01.2024

Their least-squares collocation method is based on a global covariance function. In this study, full tensor gravity gradient components have been calculated from surface gravity anomaly data collected over Southern Oklahoma region. The purpose is to show the modelling method along with covariance matrices and evaluate it using real airborne gravity gradiometry survey data and EGM08 model.

## 2. Materials and Methods

Most common measurement in geophysics and geodesy is acceleration of gravity which is the first vertical derivatives of gravity potential, $W$. The gravity potential is approximated by normal gravity field, $U$ which is generated by an ellipsoid of revolution called normal ellipsoid rotating with the earth and including its mass. The normal gravity field and its gradients are known for a specific ellipsoid such as GRS80 or WGS84. The residual part is called disturbing potential, $T$ and defined by subtracting the normal gravity potential from the total gravity potential [13].

$$T = W - U \tag{1}$$

In a local Cartesian coordinate system $(x, y, z) \rightarrow (x_1, x_2, x_3)$, the gravity gradient disturbances being second order partial derivative of the disturbing potential, $\Gamma = [\Gamma_{j,k}], j, k$ =1,2,3 is defined by [14]

$$\Gamma = \frac{\partial^2 T}{\partial x_j \partial x_k} = \begin{bmatrix} \frac{\partial^2 T}{\partial x_1 \partial x_1} & \frac{\partial^2 T}{\partial x_1 \partial x_2} & \frac{\partial^2 T}{\partial x_1 \partial x_3} \\ \frac{\partial^2 T}{\partial x_2 \partial x_1} & \frac{\partial^2 T}{\partial x_2 \partial x_2} & \frac{\partial^2 T}{\partial x_2 \partial x_3} \\ \frac{\partial^2 T}{\partial x_3 \partial x_1} & \frac{\partial^2 T}{\partial x_3 \partial x_2} & \frac{\partial^2 T}{\partial x_3 \partial x_3} \end{bmatrix} \tag{2}$$

### 2.1. Least-squares collocation

Estimating gravity gradients from surface gravity anomalies is depend on solutions to the geodetic boundary value problem. Least-Squares Collocation is one method for the solution to the boundary value problem to solve disturbing potential, $T$. Using this solution to the disturbing potential, other gravimetric quantities can be expressed as linear functional of the disturbing potential, $T$. The minimum norm, minimum error variance least-squares collocation solution for the disturbing potential is given by [15]

$$\hat{T} = C_{T,s_2}\left(C_{s_2,s_2} + D_n\right)^{-1}\ell \tag{3}$$

where observation vector (gravity anomalies) is given by $\ell = s_2 + n$ , $n$ observation noise vector, $D_n$ is observational noise, $C_{s_2,s_2}$ is the covariance matrix of observed quantities, $C_{T,s_2}$ is covariance matrix between the observed quantities and the disturbing potential.

In plane approximation, gravity disturbance is equal to gravity anomaly, which is negative vertical derivative of the disturbing potential [14]

$$\Delta g = \delta g = -\frac{\partial T}{\partial x_3} \tag{4}$$

By applying linear operators $L_1 = \partial^2/\partial x_j \partial x_k$ and $L_2 = -\partial/\partial x_3$ to the disturbing potential in equation 3, $s_2 = L_2 T$ , the least-squares solution to the gradient disturbances are given by

$$\Gamma_{jk} = C_{(\Gamma_{jk},\Delta g)}\left(C_{(\Delta g,\Delta g)} + D_n\right)^{-1}\Delta g \tag{5}$$

Covariances related to the gravity gradient disturbances can be derived by applying law of error propagation of covariance model defined for the disturbing potential [16]. Assuming a stochastic process of the disturbing potential, covariance model for the disturbing potential is based on reciprocal distance model and given by [1]

$$C_{TT}(s; x_3, x_3') = \frac{\sigma^2}{\sqrt{\alpha^2 s^2 + \left(1 + \alpha(x_3 + x_3')\right)^2}} \tag{6}$$

where $s = \sqrt{\Delta x_1^2 + \Delta x_2^2}$; $\Delta x_1 = x_1 - x_1'$; $\Delta x_2 = x_2 - x_2'$ are coordinate differences; $x_3$, $x_3'$ are heights of the points; and $\sigma^2$, $\alpha$ are covariance model parameters. Since $T$ is a potential, its covariance function enables to be upward-continued by the sum of altitude coordinates, $x_3 + x'_3$. The covariance function is based on assumption of ergodicity and thus stationary which means that the covariance function depends only on horizontal coordinate differences. By applying law of propagation of covariances to the equation (6), covariances between the gravity anomaly and the gravity gradient disturbances are derived by [1]

$$C_{(\Delta g,\Delta g)} = \frac{3\sigma^2\alpha^2}{M^{5/2}}(2\beta^2 - \alpha^2 s^2) \tag{7}$$

$$C_{(\Gamma_{11},\Delta g)} = -\frac{3\sigma^2\alpha^3\beta}{M^{7/2}}(-\beta^2 - \alpha^2 s^2 + 5\alpha 2\Delta x_1^2) \tag{8}$$

$$C_{(\Gamma_{22},\Delta g)} = -\frac{3\sigma^2\alpha^3\beta}{M^{7/2}}(-\beta^2 - \alpha^2 s^2 + 5\alpha 2\Delta x_2^2) \tag{9}$$

$$C_{(\Gamma_{33},\Delta g)} = \frac{3\sigma^2\alpha^3\beta}{M^{7/2}}(-2\beta^2 + 3\alpha^2 s^2) \tag{10}$$

$$C_{(\Gamma_{13},\Delta g)} = \frac{3\sigma^2\alpha^4\Delta x_1}{M^{7/2}}(-4\beta^2 + \alpha^2 s^2) \tag{11}$$

$$C_{(\Gamma_{12},\Delta g)} = -\frac{15\sigma^2\alpha^5\beta}{M^{7/2}}\Delta x_1 \Delta x_2 \tag{12}$$

$$C_{(\Gamma_{23},\Delta g)} = \frac{3\sigma^2\alpha^4\Delta x_2}{M^{7/2}}(-4\beta^2 + \alpha^2 s^2) \tag{13}$$

where $\beta = 1 + \alpha(x_3 + x_3')$ and $M = \beta^2 + \alpha^2 s^2$.

Using the covariance function for the disturbing potential, [14] estimates geoid undulation from the gravity anomaly data given along track in frequency domain.

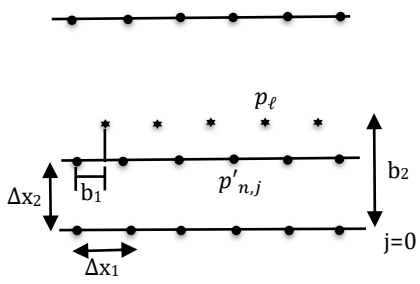


**Figure 1**. Geometry of the data points adapted from [14]

Here the problem is adapted to estimate the gravity gradient disturbances in space domain. Suppose that there are regularly distributed points along tracks being parallel each other and

having coordinates, $p'_{n,j} = (n\Delta x_1, j\Delta x_2)$, where $\Delta x_1$ is the distance between points along tracks, $n$ is number of points along tracks, $n = 0, \ldots . N-1$, $\Delta x_2$ is the distance between tracks and the number of tracks is denoted by $j = 0, \ldots . , J-1$. The gradient disturbances are estimated at the points located at $p_\ell = (\ell \Delta x_1 + b_1, b_2)$. The computation points have same along distance with observation points, but they have displacement from the j=0 track and from measurements along tracks. The displacement vector is defined by $\boldsymbol{b} = (b_1\ b_2)^T$. Observations are collected in $J \times 1$ vector including n$^{th}$ measurement along all tracks,

$$\Delta g_n = [\Delta g(p'_{n,0}) \quad \cdots \quad \Delta g(p'_{n,J-1})]^T \tag{14}$$

The cross- covariance matrix is defined by

$$C_{\Delta g,\Gamma_{j,k}}(p,p') = \\ = \begin{bmatrix} C_{\Delta g,\Gamma_{j,k}}(p_\ell,p'_n) & C_{\Delta g,\Gamma_{j,k}}(p_\ell,p'_{n+1}) & \cdots \\ C_{\Delta g,\Gamma_{j,k}}(p_{\ell+1},p'_n) & C_{\Delta g,\Gamma_{j,k}}(p_{\ell+1},p'_n) & \cdots \\ \vdots & \vdots & \vdots \end{bmatrix} \tag{15}$$

where $C_{\Delta g,\Gamma_{j,k}}(p_\ell,p'_n)$ includes $1 \times J$ row vectors that represent elements of covariances between estimation point located at $p_\ell$ and the elements of $\Delta g_n$ located at $p'_n$ . Auto-covariance matrix is defined by

$$C_{\Delta g,\Delta g}(p',p') = \\ = \begin{bmatrix} C_{\Delta g,\Delta g}(p'_m,p'_n) & C_{\Delta g,\Delta g}(p'_m,p'_{n+1}) & \cdots \\ C_{\Delta g,\Delta g}(p'_{m+1},p'_n) & C_{\Delta g,\Delta g}(p'_{m+1},p'_n) & \cdots \\ \vdots & \vdots & \vdots \end{bmatrix} \tag{16}$$

where $C_{\Delta g,\Delta g}(p'_m,p'_n)$ includes $J \times J$ matrices that represent covariances among elements of $\Delta g_n$ and $\Delta g_m$ located at track points, $p'_n$ and $p'_m$.

## 3. Results and Dicussion

The study area lies in the Wichita uplift region of the Southern Oklahoma Aulacogen that is characterized by a failed rift arm located in Oklahoma and Texas region in US [17]. The region is bounded by major fault zones to the south, Waurika Munster - North Fork-Altus-Burch faults that separate the uplift from Hollis basin and to the north, Mountain view fault and Meers fault are the major fault segments that separate the uplift from Anadarko basin (figure 2) [18].

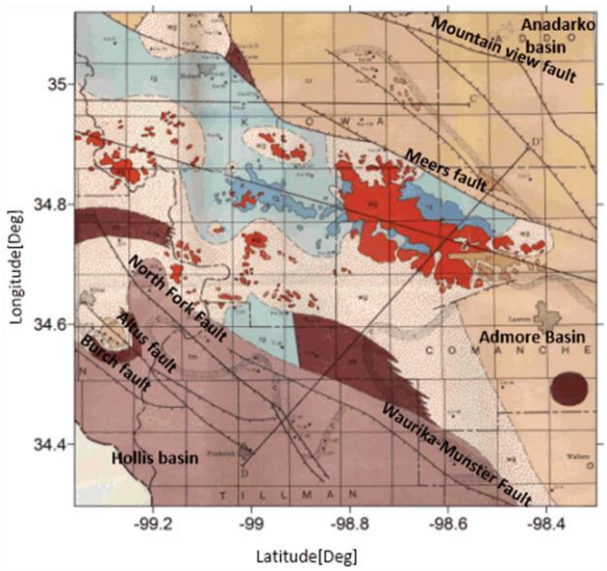


**Figure 2**. Geologic map of the Wichita uplift region extracted from map (plate I) by [18]

Many seismic studies have been performed in the area due to bearing one of major oil fields in the US. The region is also special in terms of having strong gravity signatures with moderate terrain effects. Therefore, the first gravity gradiometer survey system (GGSS) was flown over Texas/Oklahoma region in 1987 which allows the aircraft to fly low on the ground [19].

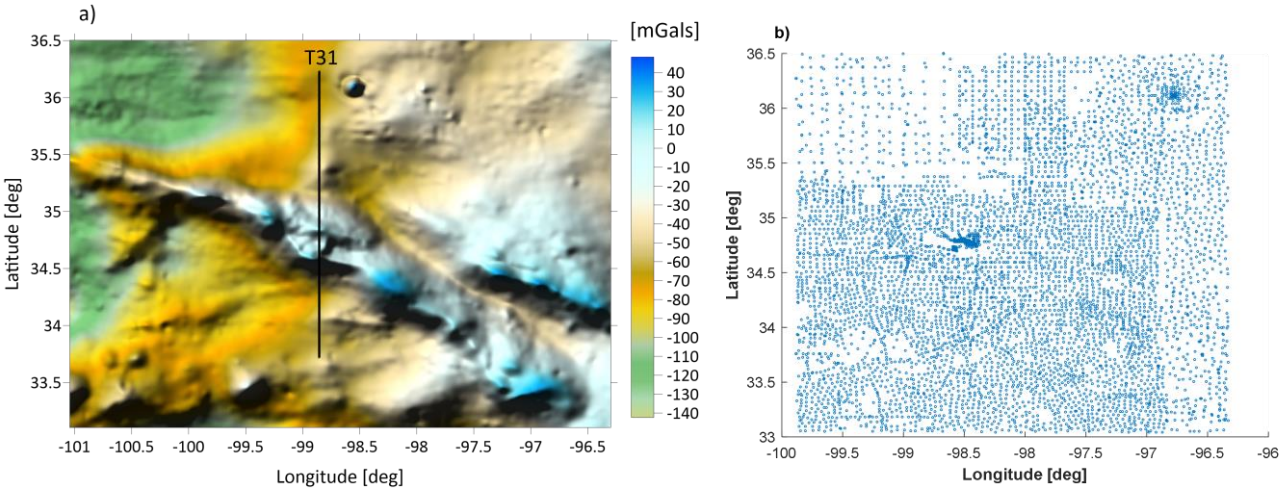


The elevation of the topography in the region (Figure 3.d) ranges from 148 m to 786 m. The mean elevation of the area is 395m. Figure 3.a demonstrates complete Bouguer gravity anomaly data of the region that are downloaded from USGS website and the real airborne gradiometric survey profile superimposed on it. The data set that generates the complete Bouguer anomaly grid was compiled from the gravity databases obtained from the National Geophysical Data Center and from the USGS and from several university theses. The data were interpolated to a 2km × 2km regular grid data. Figure 3.c demonstrates the Complete Bouguer gravity anomaly data along track T31. The region has gravity highs (50-80 mGal) trending south-east to north-west with an elongated structure. [20] indicates that these gravity highs are assumed to be caused by density variations in the upper crust.

The region also has the second largest gravity anomaly after the mid- continent rift in the US. Modeled gravity gradient disturbances are computed along profile T31 from free air gravity anomalies (Figure 3.e).

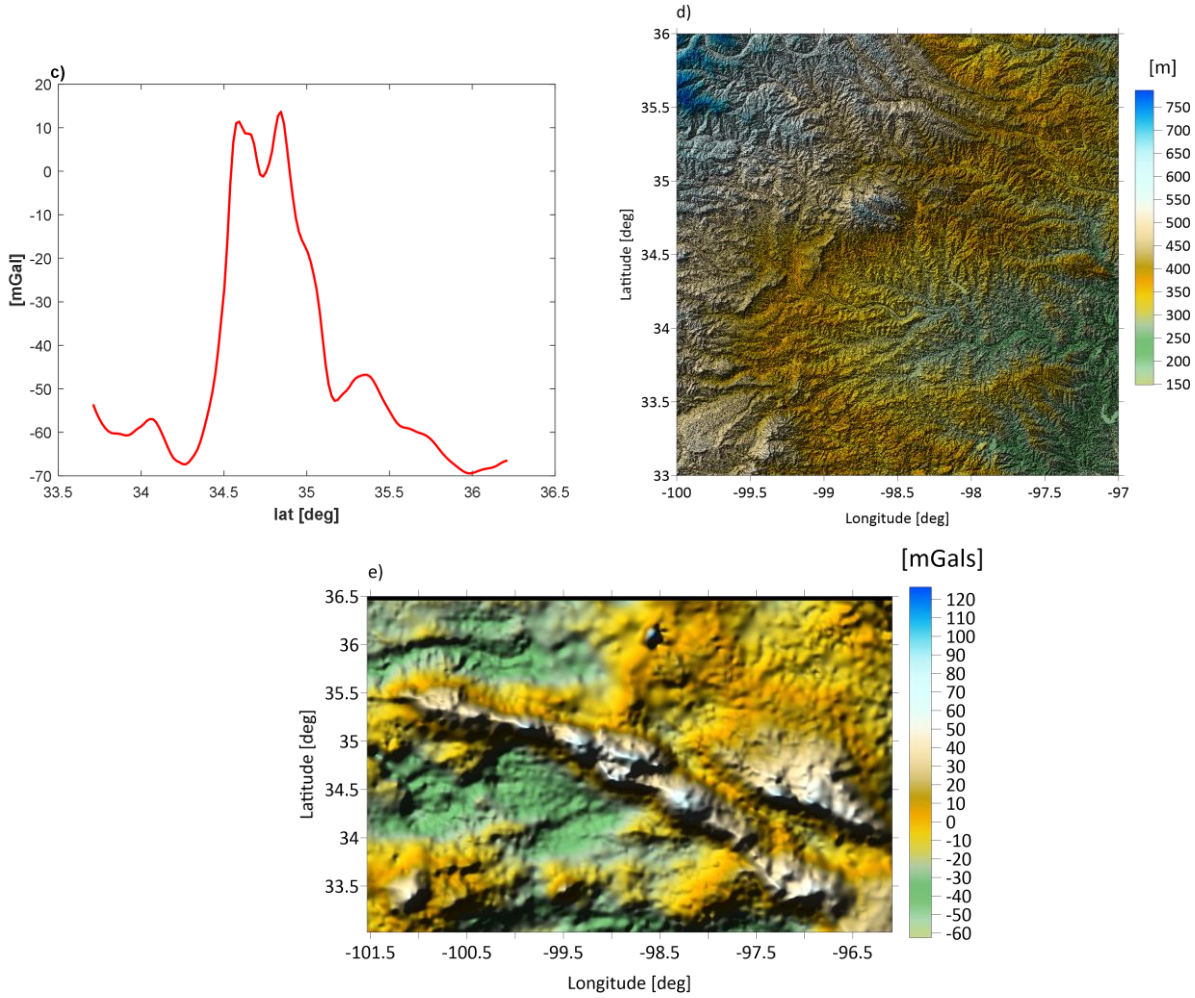


**Figure 3.**a) Complete Bouguer gravity anomaly map of Southern Oklahoma downloaded from USGS website (https://pubs.usgs.gov/ds/2006/232/data/) b) Gravity anomaly data distribution of the Wichita uplift region c) Complete Bouguer gravity anomaly along track T31 d) Topographic map of the area generated from shuttle radar topography mission (SRTM) e) Free air gravity anomaly data of the region.

**Table 1.** Reciprocal distance PSD parameters.

| j | $\sigma^2$[m⁴/s⁴] | $\alpha$[1/m] |
|---|---|---|
| 1 | $2\times10^{-5}$ | $10^{-3}$ |
| 2 | $10^{-4}$ | $6\times10^{-4}$ |
| 3 | $7.5\times10^{-4}$ | $3\times10^{-4}$ |
| 4 | $1.42\times10^{-2}$ | $1.51\times10^{-4}$ |
| 5 | $7.5\times10^{-1}$ | $4.5\times10^{-5}$ |
| 6 | $3.6\times10^{1}$ | $1.45\times10^{-5}$ |
| 7 | $7.78\times10^{2}$ | $4.9\times10^{-6}$ |
| 8 | $3.5\times10^{3}$ | $7.7\times10^{-7}$ |
| 9 | $1.1\times10^{5}$ | $4.16\times10^{-7}$ |

Covariance model parameters, $J$, $\sigma_j^2$ , $\alpha_j$ are determined from by fitting empirical determination of power spectral density (PSD) of the gravitational field data [15]. One set of model parameters derived in Texas/Oklahoma region is given in Table 1.

As shown in Figure 3.a), a single track(T31) gravity anomaly data is given between latitudes $33.71^o \leq \phi \leq 36.21^o$ and longitude at $\lambda = -98.8635^o$. Modeled gradients are computed on the points along this track. The length of the observation track(T31) is about 278 km including $N$ =140 points. Along track distance between points is about 2 km. To compute gradient disturbances on the ground level, the altitude of points is set to zero, $x_3 = x'_3 = 0$. It is assumed that the observations are uncorrelated and have equal variance. The accuracy of the gravity anomaly data is taken as 2mGal. Therefore, covariance matrix of the observation noise becomes a diagonal matrix of size $140 \times 140$, with variances of $4mGal^2$ .

$$D_n = \begin{bmatrix} 4mgal^2 & 0 & 0 \\ 0 & \ddots & 0 \\ 0 & 0 & 4mgal^2 \end{bmatrix}_{140\times140}$$

Since the estimation points are on the observation profile, the displacement vector $\boldsymbol{b} = 0$. In case of a single track, J=1 and $\Delta x_2 = 0$. The auto- and cross- covariance matrices given in equations (15) and (16) take the form of,

$$C_{\substack{\Delta g,\Delta g \\ 140\times140}}(p,p') = \begin{bmatrix} C(p_1,p'_1) & \cdots & C(p_1,p'_n) \\ \vdots & \ddots & \vdots \\ C(p_\ell,p'_1) & \cdots & C(p_\ell,p'_n) \end{bmatrix} \quad (17)$$

$$C_{\substack{\Gamma_{jk},\Delta g \\ 140\times140}}(p,p') = \begin{bmatrix} C(p_1,p'_1) & \cdots & C(p_1,p'_n) \\ \vdots & \ddots & \vdots \\ C(p_\ell,p'_1) & \cdots & C(p_\ell,p'_n) \end{bmatrix} \quad (18)$$

According to equations (7)-(13), cross-covariances $C_{(\Gamma_{11},\Delta g)}$, $C_{(\Gamma_{22},\Delta g)}$, $C_{(\Gamma_{12},\Delta g)}$ and $C_{(\Gamma_{23},\Delta g)}$ become zero. Remaining covariances along track T31 are demonstrated in Figure 4.

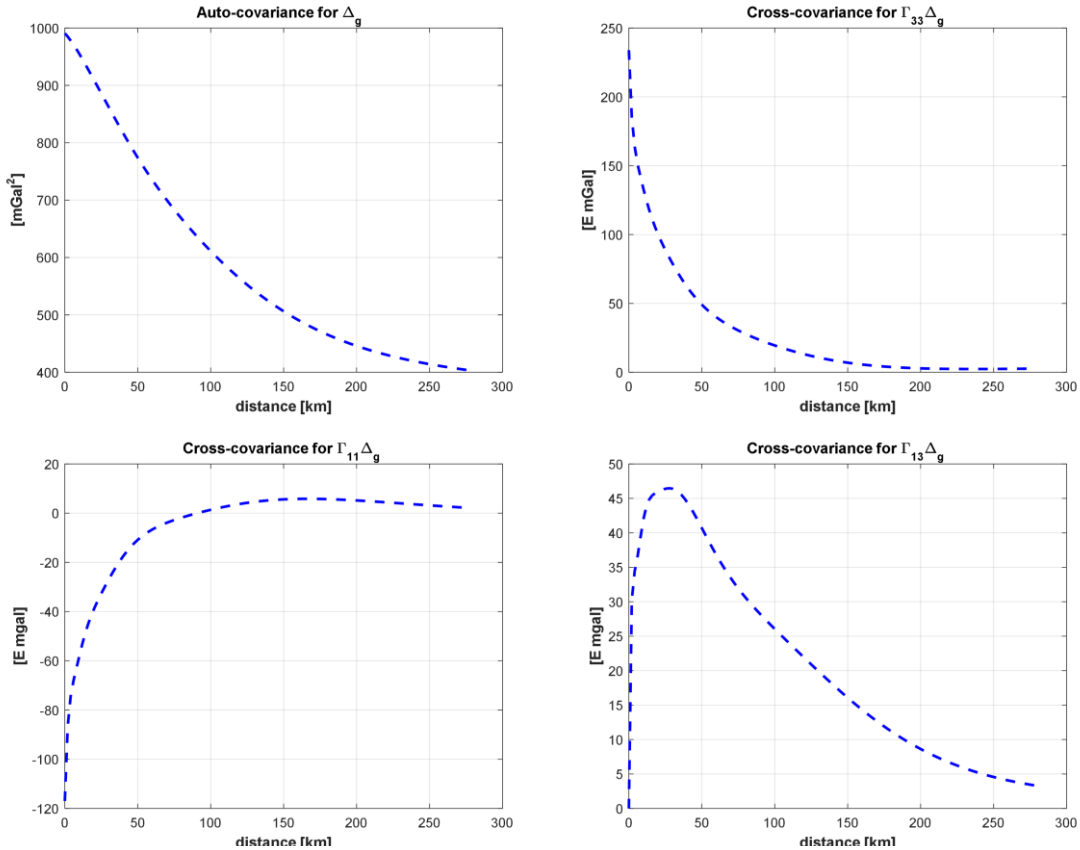


**Figure 4.** Auto-covariance for the gravity anomaly, $\Delta g$ ,and cross-covariances between the gravity gradient disturbances, $\Gamma_{33}$ , $\Gamma_{11}$ and $\Gamma_{13}$, and the gravity anomaly, $\Delta g$.

Using these covariances, the modeled gravity gradient disturbances are computed using least-squares collocation by

$$\underset{140\times1}{\Gamma_{jk}} = \underset{140\times140}{C_{(\Gamma_{33},\Delta g)}} \left( \underset{140\times140}{C_{(\Delta g,\Delta g)}} + \underset{140\times140}{D_n} \right)^{-1} \underset{140\times1}{\Delta g} \quad (19)$$

and compared with the observation profile generated from EGM08 model. The resolution of the EGM08 model ($n_{max}$= 2160) is about 9 km at the equator [21]. East-west resolution of EGM08 model for this region is about 7.6 km. The results are illustrated in Figure 5.

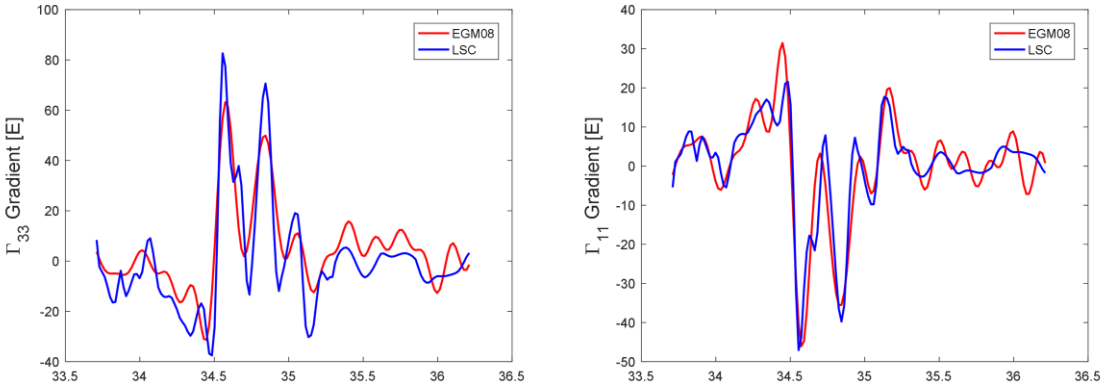

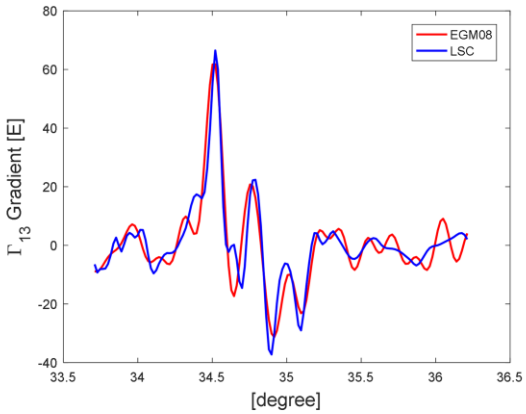


**Figure 5.** Plots of modeled gravity gradient disturbances computed on the earth's surface using least-squares collocation (LSC) and corresponding EGM08 profile along track T31.

To estimate the gravity gradient disturbances from multiple observation tracks, additional two tracks are considered given either side of the track (T31) between latitudes $33.71^o \leq \phi \leq 36.21^o$and longitudes at $\lambda = -98.9294^o$ and $\lambda = -98.7976^o$. Along track distance is same for all tracks, $\Delta x_1 = 2km$ and the distance between tracks is $\Delta x_2 = 6km$. For three tracks, $J = 3$. Each element of cross-covariance matrix, which is $140 \times 420$ in size, contains $1 \times 3$ row vectors. Cross-covariances are defined by

$$\underset{140\times420}{C_{\Gamma_{jk},\Delta g}(p,p')} = \begin{bmatrix} \underset{1\times3}{C(p_1,p'_1)} & \underset{1\times3}{C(p_1,p'_2)} & \underset{1\times3}{C(p_1,p'_3)} & \iddots \\ \underset{1\times3}{C(p_2,p'_1)} & \underset{1\times3}{C(p_2,p'_2)} & \underset{1\times3}{C(p_2,p'_3)} & \cdots \\ \cdots & \vdots & \vdots & \cdots \\ \underset{1\times3}{C(p_\ell,p'_n)} & \underset{1\times3}{C(p_\ell,p'_n)} & \underset{1\times3}{C(p_\ell,p'_n)} & \ddots \end{bmatrix} \quad (20)$$

The elements of the covariance matrix represent the covariances between the gravity gradient disturbances on the middle track and gravity anomalies given on the three tracks. Elements of the auto-covariance matrix are the covariances between gravity anomalies on any two tracks separated by $0km$, $\Delta x_2 km$ and $2\Delta x_2 km$ and given by

$$\underset{420\times420}{C_{\Delta g,\Delta g}(p',p')} = \begin{bmatrix} \underset{3\times3}{C(p'_1,p'_1)} & \underset{3\times3}{C(p'_1,p'_2)} & \underset{3\times3}{C(p'_1,p'_3)} & \iddots \\ \underset{3\times3}{C(p'_2,p'_1)} & \underset{3\times3}{C(p'_2,p'_2)} & \underset{3\times3}{C(p'_2,p'_3)} & \cdots \\ \cdots & \vdots & \vdots & \cdots \\ \underset{3\times3}{C(p'_n,p'_1)} & \underset{3\times3}{C(p'_n,p'_2)} & \underset{3\times3}{C(p'_n,p'_n)} & \ddots \end{bmatrix} \quad (21)$$

And corresponding observation vector includes gravity anomalies on the three tracks and is defined by

$$\underset{420\times1}{\Delta g}\ [\Delta g(p'_{n,0}) \quad \Delta g(p'_{n,1}) \quad \Delta g(p'_{n,2}) \quad \cdots]^T \quad (22)$$

Figure 6 illustrates a comparison of modeled gravity gradient disturbances estimated using LSC with corresponding EGM08 data profile. Modeled gravity gradient disturbances agree well with the EGM08 generated gravity gradient disturbances. There is some discrepancy between gradients that include components in the east-west direction and corresponding EGM08 data profile, especially for $\Gamma_{22}$ gradient. The discrepancy could be due to a lack of data in $x_2$-direction. Improving the estimation of the modeled gradient, $\Gamma_{22}$ could be achieved by adding more data tracks to the estimation process.

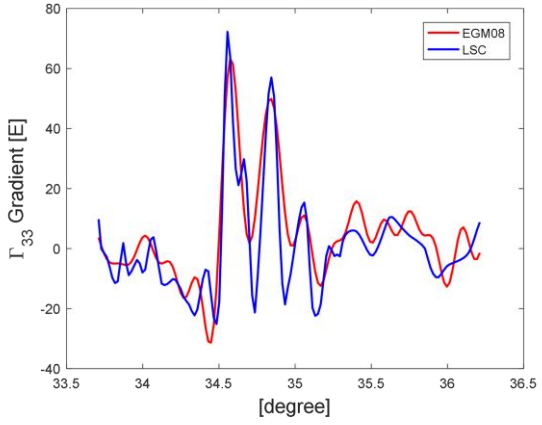


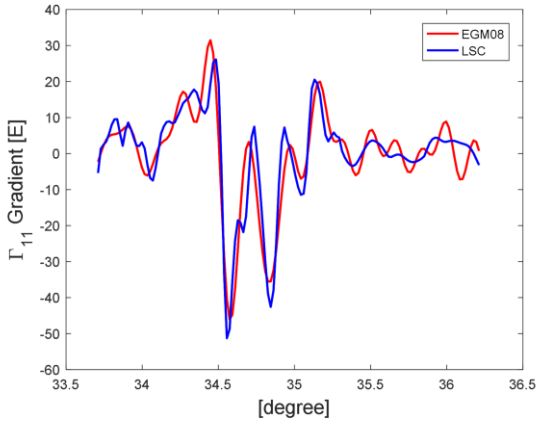

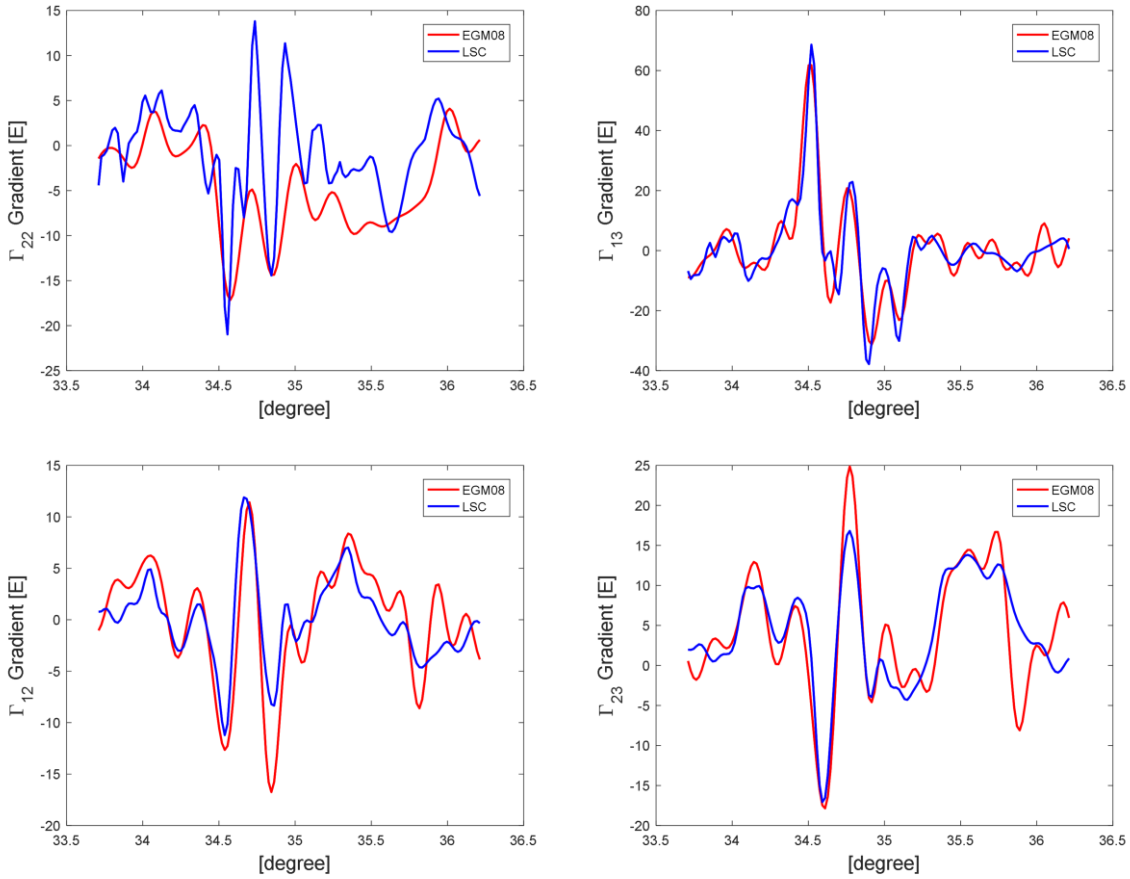


**Figure 6.** Computed gravity gradient disturbances on the earth's surface (zero altitude) using LSC and corresponding EGM08 gradients along track T31.

Figure 7 illustrate differences between modeled gravity gradient disturbances and EGM08 generated gradients along profile T31. The corresponding statistics of the differences are listed in table 2. Standard deviation of the differences ranges from 3 E to 10 E. Standard deviation of $\Gamma_{22}$ is smaller than that of the other diagonal gradients as magnitude of $\Gamma_{22}$ gradient is smaller compared to the other diagonal gradients. Overall, standard deviation of differences in gradients that include components in the east-west direction is also smaller than that of the other gradients. Finally, modeled gravity gradient disturbances are computed at an aircraft altitude along track T31 and compared with the real airborne gravity gradiometry data as well. The profile T31 is an actual gravity gradiometry survey data and is approximately 278 km long. The altitude of the profile above terrain is approximately 1000m. The profile includes 2533 points with a sampling interval of 110 m. [17] stated that terrain effect on profile T31 is negligible; so, terrain correction hasn't been applied to the profile. Some of the gradients along this track are illustrated in Figure 8.

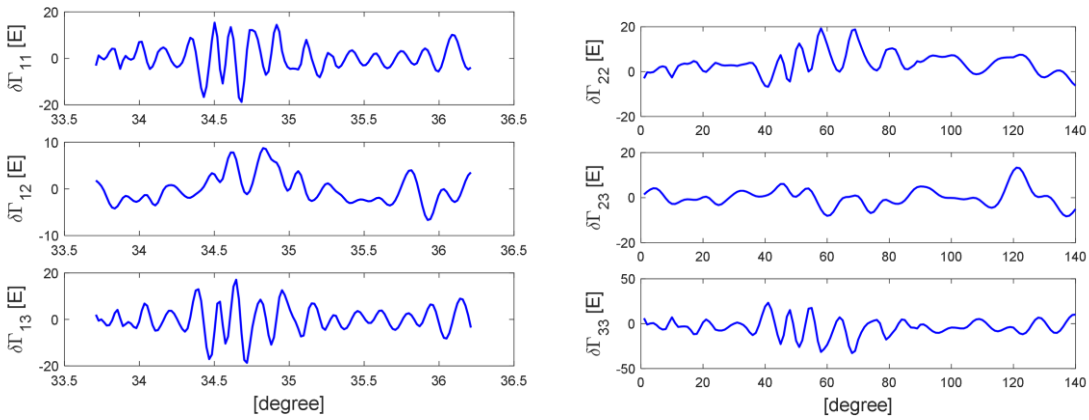


**Figure 7.** Differences between modeled gravity gradient disturbances and EGM08 gradients along track T31.

**Table 2.** Differences between modeled gradient disturbances and EGM08 gradients along profile T31 and corresponding statistics

| Gradients [E] | $\delta\Gamma_{11}$ | $\delta\Gamma_{12}$ | $\delta\Gamma_{13}$ | $\delta\Gamma_{22}$ | $\delta\Gamma_{23}$ | $\delta\Gamma_{33}$ |
|---|---|---|---|---|---|---|
| Mean | 0.320 | -0.05 | 0.105 | 3.640 | 0.179 | -3.961 |
| Std | 5.936 | 3.143 | 6.034 | 4.870 | 3.996 | 9.528 |
| max | 15.360 | 8.738 | 17.095 | 19.284 | 13.331 | 23.377 |
| min | -18.753 | -6.663 | -18.684 | -6.745 | -8.291 | -32.771 |

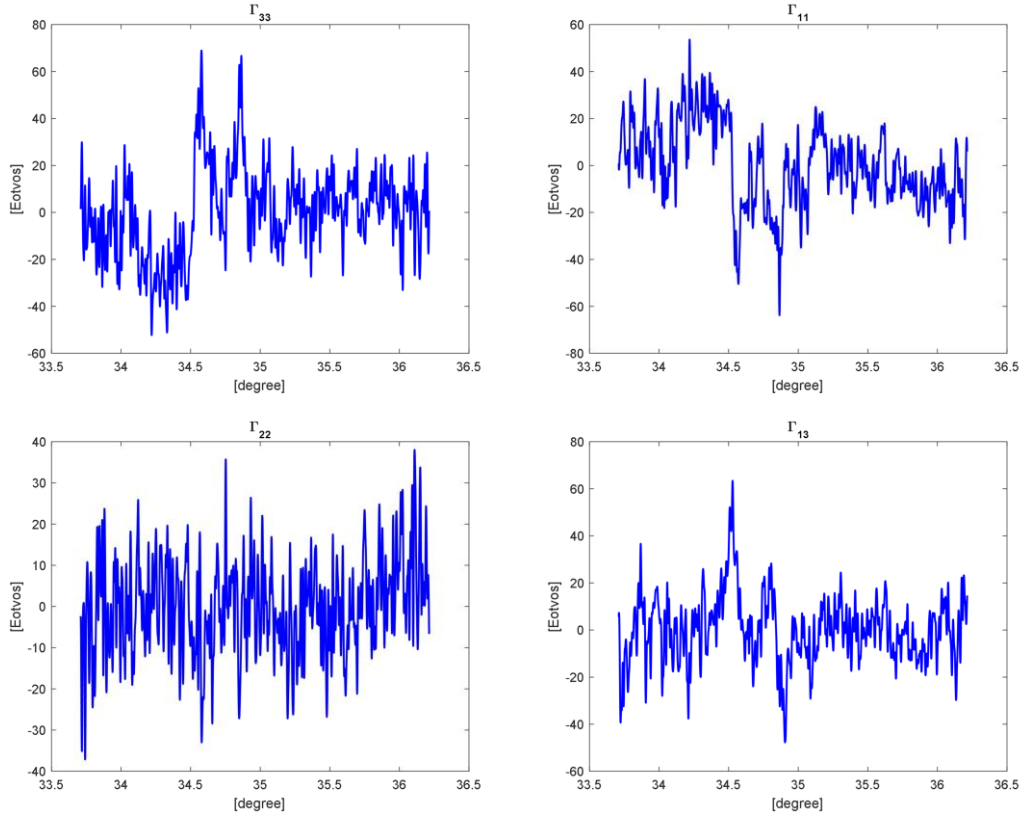


**Figure 8.** Gravity Gradiometer Survey Data along T31 profile

GGSS data are smoothed with a window size of 10 km to reduce very high frequency variations. Modeled gradient disturbances are calculated at the aircraft altitude of $x_3 = x'_3 = 1000m$. Since GGSS data has higher resolution, estimation points are spaced 0.11km apart. Therefore, the displacement vector components are $b_1 = 0.11$km and $b_2 = 0$.The results are illustrated in Figure 10. Modeled gradients generally agree with EGM08 model generated gradients. However, there are some discrepancies observed between airborne gradiometric data and some modeled gradients. The modeled gradients, $\Gamma_{22}$ and $\Gamma_{12}$ have more agreement with EGM08 data than the airborne data. Since being first test of the Gravity Gradiometer Survey System (GGSS) performed in 1987, the data does not meet highest quality standards. Figure 9 compares spectra of both GGSS data and corresponding EGM08 profile for the gradient $\Gamma_{12}$ along track T31.Power spectral density of GGSS data does not agree much with PSD of EGM08 data. Figure 11 demonstrates differences between modeled gravity gradient disturbances and EGM08 generated gradients together with airborne gradiometer data along track T31.

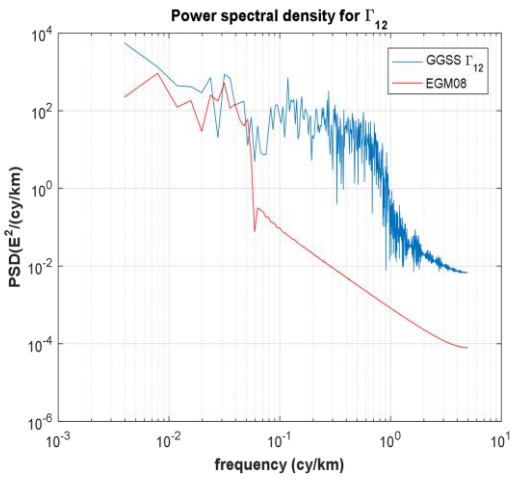


**Figure 9.** Power spectral densities of $\Gamma_{12}$ according to EGM08 model and GGSS data along track T31.

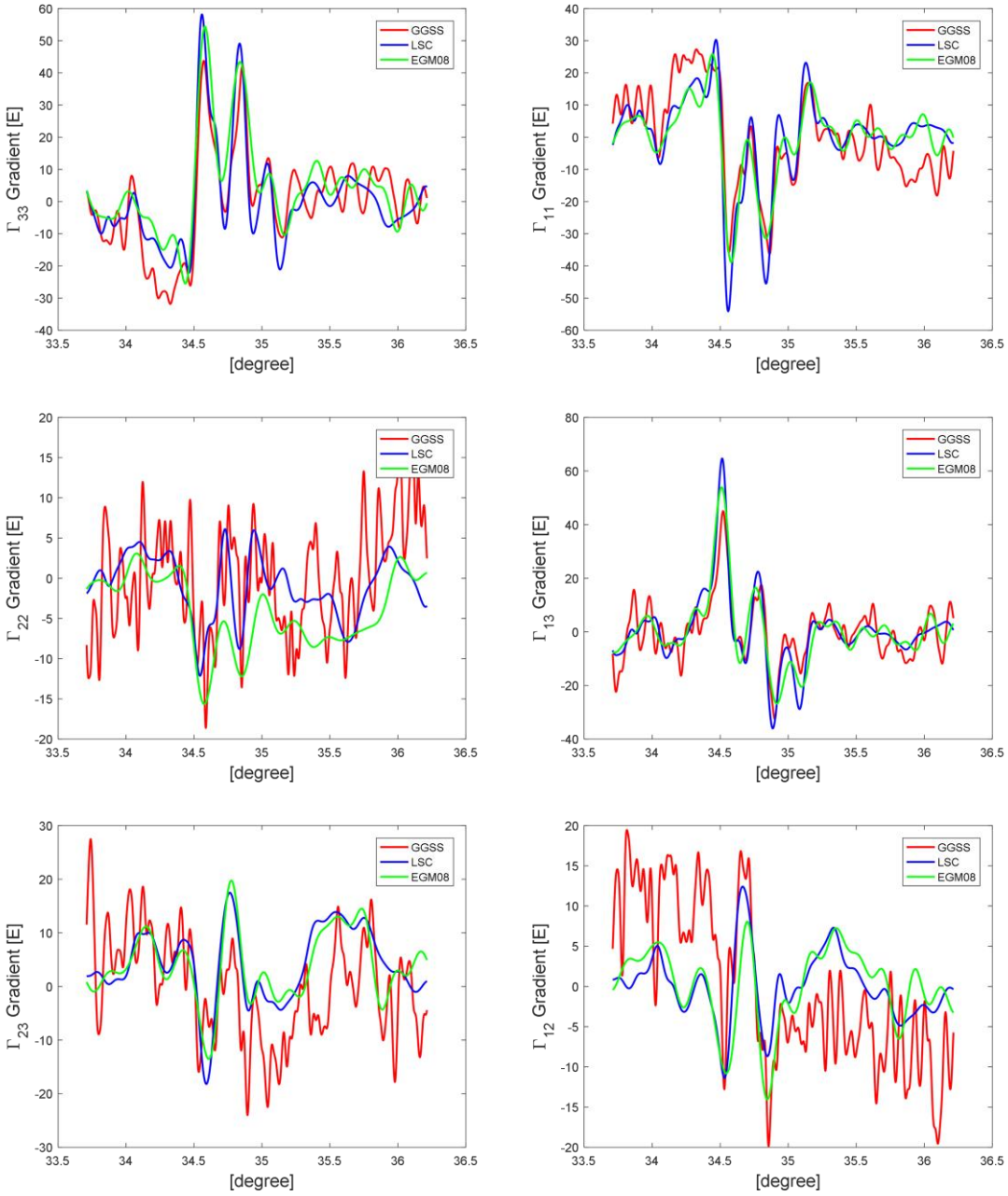


**Figure 10.** Plots of modeled gravity gradient disturbances, EGM08 gradients and airborne gradiometry data along track T31

Tables 3 and 4 show differences between modeled gradient disturbances and EGM08 gradients, as well as airborne gradiometry data along track 31. Standard deviation of differences based on airborne gradiometry data is greater than those calculated from EGM08 data. In most cases, standard deviation of differences between modeled gradients with components in the east-west direction and both EGM08 gradients and airborne gradiometer data is smaller than that of the other gradients.

**Table 3.** Differences between modeled gradient disturbances and EGM08 gradients along profile T31 and corresponding statistics

| Gradients [E] | $\delta\Gamma_{11}$ | $\delta\Gamma_{12}$ | $\delta\Gamma_{13}$ | $\delta\Gamma_{22}$ | $\delta\Gamma_{23}$ | $\delta\Gamma_{33}$ |
|---|---|---|---|---|---|---|
| Mean | 0.437 | -0.041 | 0.120 | 3.250 | 0.291 | -3.671 |
| Std | 5.766 | 2.928 | 4.907 | 3.329 | 3.055 | 6.283 |
| max | 16.484 | 10.546 | 11.288 | 12.775 | 9.417 | 11.496 |
| min | -21.400 | -5.484 | -14.296 | -4.150 | -7.031 | -26.037 |

**Table 4.** Differences between modeled gradient disturbances and airborne gradiometry data along profile T31 and corresponding statistics

| Gradients [E] | $\delta\Gamma_{11}$ | $\delta\Gamma_{12}$ | $\delta\Gamma_{13}$ | $\delta\Gamma_{22}$ | $\delta\Gamma_{23}$ | $\delta\Gamma_{33}$ |
|---|---|---|---|---|---|---|
| Mean | 0.188 | 0.016 | 0.373 | -0.893 | 4.159 | 0.729 |
| Std | 9.107 | 8.983 | 7.249 | 6.411 | 8.898 | 8.250 |
| max | 21.160 | 16.890 | 24.556 | 13.615 | 21.087 | 21.084 |
| min | -22.328 | -19.564 | -16.323 | -18.326 | -25.443 | -17.942 |

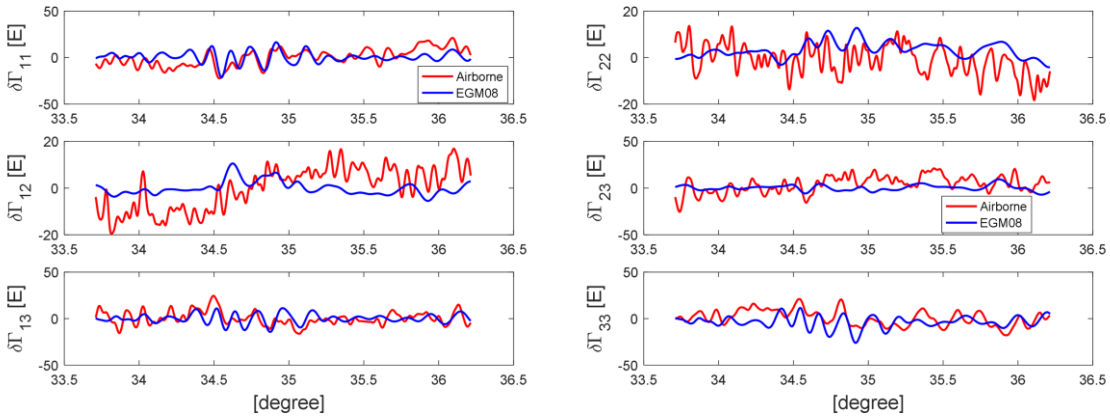


**Figure 11.** Differences between modeled gravity gradient disturbances and both EGM08 gradients and airborne gradiometry data along profile T31.

## 4. Conclusions

This study presents modeling of the gravity gradient disturbances from free air gravity anomaly data employing least-squares collocation and evaluates the modeling method using both real airborne gradiometer data and EGM08 gradients. Such modeling is useful for validating airborne gradiometer survey data. It has been shown that modeled gradients have good agreement with EGM08 generated gravity gradient disturbances both on the ground and at an aircraft altitude. There are some discrepancies in modeled gradients including components in the east-west direction, which may be due to a lack of data in that direction. Since the airborne gradiometry data used in this study is the first test survey of airborne gradiometer survey system, the quality of the data may not be good enough to evaluate all modeled gradients. It is important to emphasize that the airborne gradiometer data has higher resolution than both EGM08 model and ground gravity anomaly data. Standard deviation of differences between modeled gradients and both EGM08 gradients and airborne gradiometer data are between 2-10E for all gradients. The differences in gradients containing components in the east-west direction are smaller than those in the other gradients, likely because these gradients have smaller magnitude than the others. This can be attributed to elongated structure of the fault system lying in this region, resulting in less variations in gradients along the east-west direction.

### Ethics committee approval and conflict of interest statement

This article does not require ethics committee approval.

This article has no conflicts of interest with any individual or institution.

### Acknowledgment

The author thanks two anonymous reviewers for their valuable comments on this manuscript.

### Author Contribution Statement

S. Uzun conceptualized the manuscript, wrote original draft, carried out numerical experiments, revised the manuscript and approved final version of the manuscript.

### References

[1] Jekeli, C. 2003. Statistical Analysis of Moving-Base Gravimetry and Gravity Gradiometry, Report No.466, Ohio State University.

[2] Jekeli, C. 2006. Airborne Gradiometry Error Analysis: Surveys in Geophysics, V.27, pp. 257-275. DOI:10.1007/s10712-005-3826-4

[3] Kohrn, B. S., Bonet, C., DiFrancesco, D. and Gibson, H. 2011. Geothermal Exploration Using Gravity Gradiometry - a Salton Sea Example: GRC transactions. V.35, pp.1699-1702.

[4] Represas P., Monteiro Santos F.A., Ribeiro. J., Ribeiro J.A., Almeida E.P., Gonçalves R., Moreira M. and Mendes-Victor L.A., 2013. Interpretation of gravity data to delineate structural features connected to low-temperature geothermal resources at Northeastern Portugal: Journal of applied geophysics, V.92, pp. 30-38. DOI: 10.1016/j.jappgeo.2013.02.011

[5] Shoffner J.D., Li Y., Sabin A. and Lazaro M., 2011. Understanding the utility of gravity and gravity gradiometry for geothermal exploration in the Southern Walker Lake Basin, Nevada: GRC Transactions, V.35, pp.1747-1751.

[6] Martinez, C., Li, Y., Krahenbuhl, R. and Braga, M. A. 2013. 3D inversion of airborne gravity gradiometry data in mineral exploration: A case study in the Quadrilatero Ferrifero, Brazil, V.78, no.1, pp. B1-B11. DOI: 10.1190/GEO2012-0106.1

[7] Mataragio, J. 2012. Exploring for Gold and Geothermal Systems in the Great Basin Using Full Tensor Gravity Gradiometry: GRC Transactions, V. 36, pp. 1009-1012.

[8] Pappa, F., Ebbing, J., Ferraccioli, F. and van der Wal, W. 2019. Modelling Satellite Gravity Gradient Data to Derive Density, Temperature and Viscosity Structure of the Antarctic Lithosphere: Journal of Geophysical Research: Solid Earth, V.124, pp. 12053-12076. DOI: 10.1029/2019JB017997

[9] Mickus, K.L. and Hinojosa, J.H. 2001. The complete gravity gradient tensor derived from the vertical component of gravity: a Fourier transform technique: Journal of applied Geophysics, V.46, pp.159-174. DOI:10.1016/S0926-9851(01)00031-3

[10] Wan, X., Annan, R.F. and Ziggah, Y.Y. 2023. Altimetry-Derived Gravity Gradients Using Spectral Method and Their Performance in Bathymetry Inversion Using Back-Propagation Neural Network: Journal of Geophysical Research: Solid Earth, V.128. DOI:10.1029/2022JB025785
[11] Jekeli, C. and Zhu, L. 2006. Comparison of methods to model the gravitational gradients from topographic data bases: Geophysical Journal International, V.166, pp.999-1014. DOI: 10.1111/j.1365-246X.2006.03063.x
[12] Jekeli, C. and Zhu, L. 2009. Gravity gradient modeling using gravity and DEM: Journal of Geodesy, V.83, pp. 557-567. DOI: 10.1007/s00190-008-0273-2
[13] Hofmann-Wellenhof, B., Moritz, H. 2005. Physical Geodesy. Springer Verlag, Berlin, 403 p.
[14] Jekeli, C. 2017. Spectral Methods in Geodesy and Geophysics: Taylor and Francis, 415 p.
[15] Jekeli, C. 2010. Least-squares Collocation, Lecture notes, School of Earth Sciences, Ohio State University.
[16] Moritz, H. 1980. Advanced Physical Geodesy, Herbert Wichmann Verlag, Karlsruhe (reprint 2008 by Division of Geodesy and Geospatial Science, School of Earth Sciences, Ohio State University), 500 p.
[17] Erkan, K. 2015. Geophysical Investigations on Gravity Gradiometry and Magnetic Data over the Wichita Uplift Region, Southwestern Oklahoma, Report No. 509, Ohio State University
[18] Ham, W.E., Denison, R.E. and Meritt, C.A. 1964. Basement rocks and structural evolution of Southern Oklahoma: Oklahoma Geological Survey Bulletin, 95, 302 p. plate I.
[19] Jekeli, C. 1993. A review of gravity gradiometer survey system data analyses: Geophysics, V.58, No:4, pp.508-514. DOI:10.1190/1.1443433
[20] Robbins, S.L. and Keller, G.R. 1992. Complete Bouguer and Isostatic residual maps of the Anadarko Basin, Wichita Mountains and surrounding areas, Oklahoma, Kansas, Texas and Colorado, US Geological Survey Bulletin, No:1866G, 11 p.
[21] Pavlis, N.K., Holmes, S.A., Kenyon, S.C., Factor, J.F. 2012. The development and evaluation of Earth Gravitational Model (EGM2008): Journal of Geophysical Research, V.117, B04406. DOI: 10.1029/2011JB008916